Influence of Global-Scale Variability on the Subtropical Ridge over Southeast Australia

WENJU CAI, PETER VAN RENSCH, AND TIM COWAN

CSIRO Marine and Atmospheric Research, Aspendale, Victoria, Australia

(Manuscript received 18 October 2010, in final form 27 April 2011)

ABSTRACT

In recent decades, southeast Australia (SEA) has experienced a severe rainfall decline, with a maximum reduction in the austral autumn season. The cause(s) of this decline remain unclear. This study examines the interaction between remote large-scale climate modes and an atmospheric phenomenon known as the subtropical ridge (STR) at the local scale. A focus is placed on the utility of using the STR as a bridge for understanding how these remote climate drivers influence SEA rainfall through a response in local atmospheric conditions. Using observational data since 1979, it is found that a strong seasonality exists in the impact of the STR on SEA rainfall. In austral autumn, because SEA rainfall is poorly correlated with the STR intensity (STRI) and STR position (STRP) on an interannual basis, it follows that most of the autumn rainfall reduction cannot be explained by the STRI changes in this season. There is also no clear relationship between the autumn STR and known remote modes of variability. Reductions in SEA rainfall have occurred in the austral winter and spring seasons; however, neither is significant. During winter, although El Niño–Southern Oscillation (ENSO) has little impact on the STR, there is a significant influence from the Indian Ocean dipole (IOD) and the southern annular mode (SAM). The IOD impact is conducted through equivalent-barotropic Rossby wave trains stemming from the eastern Indian Ocean in response to the IOD-induced anomalous convection and divergence. These wave trains modify the intensity and position of the ridge over SEA. The impact from the SAM is similarly projected onto the STRI and STRP. The STR trend accounts for the entire observed decline in SEA winter rainfall, 80% of which is contributed by the upward trend of the IOD; the SAM exhibits virtually no trend over the 30-yr period in this season. In spring, SEA rainfall shows strong interannual variability and is well correlated with the STRI; the ridge itself is influenced by the IOD and ENSO but not by the SAM. The Indian Ocean is a major pathway for ENSO's impact on SEA rainfall in this season, which is conducted by two wave trains emanating from the east and west poles of the IOD. These wave train patterns share an anomalously high surface pressure center south of Australia, which does not align with the STR over SEA. As such, only a small portion of the STRI variance is accounted for by fluctuations in ENSO and the IOD. Long-term changes in the STRI account for about 90% of the observed decline in SEA spring rainfall, all of which are due to a recent increased frequency in the number of positive IOD events (upward IOD trend); ENSO shows no long-term trend over the 30-yr period. In summary, variability and change in winter and spring rainfall across SEA can be understood through the impact of remote climate modes, such as ENSO, the IOD, and the SAM, on the STR. This approach, however, offers no utility for understanding what drives the long-term SEA autumn rainfall decline, the dynamics of which remain elusive.

1. Introduction

The subtropical ridge (STR) refers to the mean latitude of anticyclones (high pressure systems) that are found near the midlatitudes (e.g., over southern Australia in the Southern Hemisphere). The existence of the STR is a result of warm equatorial air moving poleward, forming the upper circulation branch of the Hadley cell. The air loses heat and sinks around the 30° latitude band, generating a hemispheric belt of high surface pressure. In the Southern Hemisphere, the ridge moves equatorward (north) during austral autumn [March–May (MAM)] and winter [June–August (JJA)], reaching a northernmost latitude during late winter to early spring but migrates poleward during austral spring [September–November (SON)] and summer [December–February (DJF)], arriving at a southernmost latitude in February (Fig. 1a) (Pittock 1973; Drosdowsky 2005). Thus, the intensity and position of the STR are strongly associated with the seasonal weather conditions over southern Australia.

Annual rainfall totals over regions such as southeast Australia (SEA, land points south of 33°S and east of

Corresponding author address: Wenju Cai, CSIRO Marine and Atmospheric Research, PMB 1, Aspendale VIC 3195, Australia.
E-mail: wenju.cai@csiro.au

DOI: 10.1175/2011JCLI4149.1

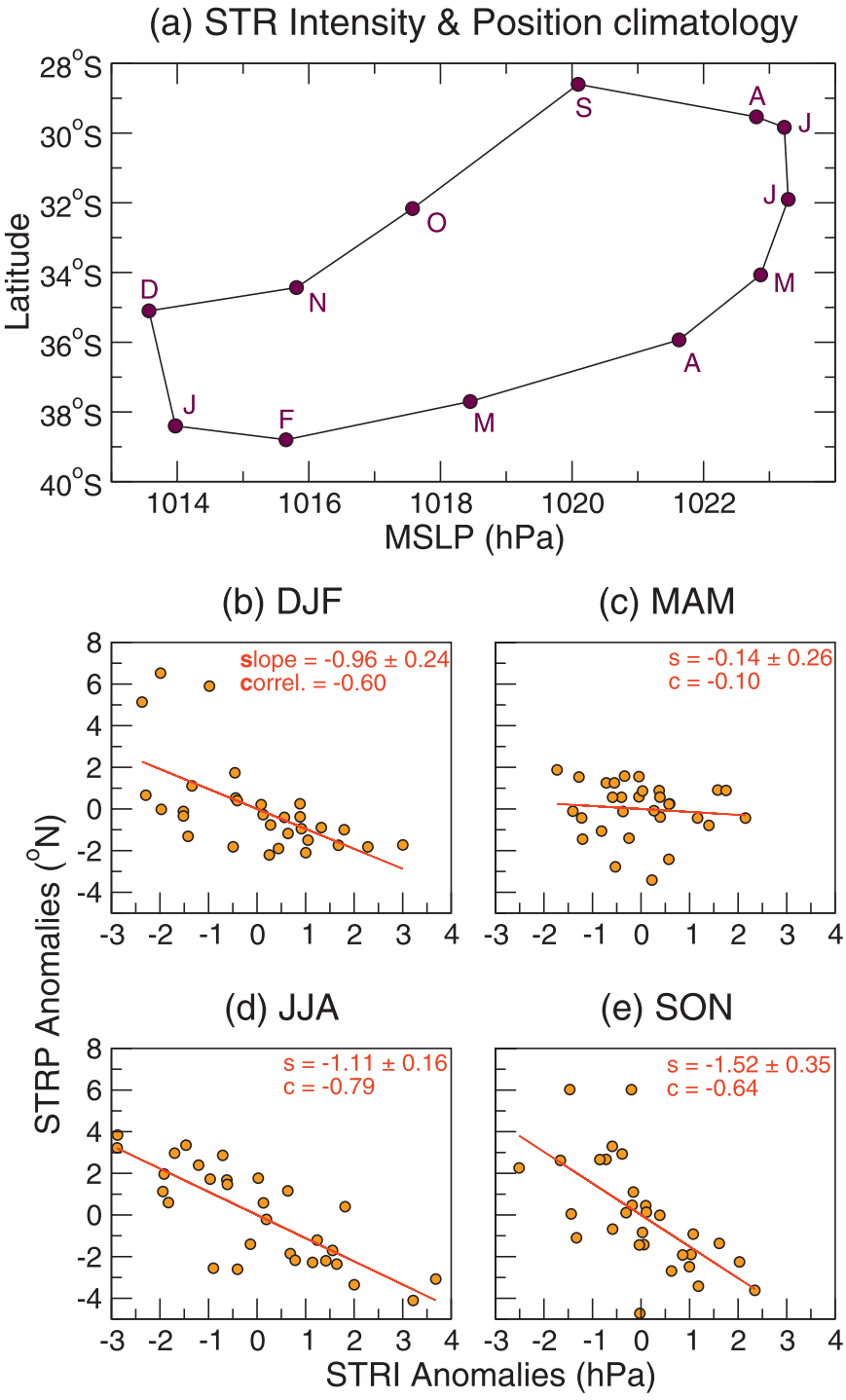

FIG. 1. (a) The annual cycle of movement and intensity of the STR, depicted as mean monthly pressure vs latitude. The month is indicated by the first letter of the name of the month. Detrended STRI vs STRP for austral (b) summer, (c) autumn, (d) winter, and (e) spring. All plots are for the period 1979–2008.

135°E) and southwest Western Australia (SWWA) have declined substantially over recent decades (Cai et al. 2003; Cai and Cowan 2006; Gallant et al. 2007; Taschetto and England 2009; Cai and Cowan 2008a; Murphy and Timbal 2008; Hope et al. 2009). For SEA, this decline is strongest in the autumn both in terms of the absolute and percentage change of the long-term mean, whereas in winter and spring the rainfall reductions are not significant (see Fig. 11, bottom panels). The reduction in SEA autumn rainfall and increase in regional temperatures have contributed to an unprecedented reduction in inflows across the southern catchment of Australia's longest river system, the Murray–Darling Basin (Cai and Cowan 2008b; Yu et al. 2010).

A key motivation of this study is to understand the STR's impact over SEA and how this is related to large-scale climate modes. Previous studies rely on two parameters to describe the property of the STR, that is, the intensity (STRI) and position (STRP) (Timbal et al. 2010 and references therein). The STRP is used to explore the impact of temporal variations in the mean latitude of the anticyclones (e.g., Pittock 1973; Gibson 1992; Drosdowsky 2005; Larsen 2008; Williams and Stone 2009). Drosdowsky (2005) constructed a STRP time series over eastern Australia (10°–44°S, 145°–150°E) based on mean sea level pressure (MSLP) from daily reanalysis and monthly observed values. Subsequent studies, using either this definition (Williams and Stone 2009) or a variation (e.g., Larsen 2008; Larsen and Nicholls 2009) suggest that there is no systematic trend in the STRP. However, the STRI, defined as the maximum MSLP across given longitudes, has been increasing (intensifying) during the twentieth century (e.g., Larsen and Nicholls 2009) and could explain up to 70% of the observed autumn to early winter (March–July) SEA rainfall decline (Timbal et al. 2007).

Given the suggested significant impact of the STRI trend, it is prudent to use the STR to understand the dynamics of the rainfall decline. Identifying factors that contribute to the variability and trend of the STR may lead to an attribution of the observed rainfall reduction. Australia's rainfall is dominated by several remote large-scale modes of climate variability, such as El Niño–Southern Oscillation (ENSO) (e.g., McBride and Nicholls 1983; Ropelewski and Halpert 1987), the Indian Ocean dipole (IOD) (e.g., Ashok et al. 2003; Cai et al. 2009a), and the southern annular mode (SAM) (e.g., Cai et al. 2003; Li et al. 2005; Cai and Cowan 2006; Hendon et al. 2007).

ENSO is known to affect the behavior of the STR in both the Northern and Southern Hemispheres by displacing the subtropical jet streams (Chen et al. 2008). During the peak of an El Niño event—that is, when the Southern Oscillation index (SOI) is highly negative—anomalous shifts in the position and strength of the local Hadley cell and Walker circulation are associated with shifts in the upper-tropospheric jet stream (Drosdowsky 2003). In the Northern Hemisphere, variations of the ridge position during ENSO cycles change the tracks of tropical cyclones (Wu et al. 2004). During El Niño events, the STR is stronger in the Southern Hemisphere and located farther equatorward than normal (Drosdowsky 2005), whereas during La Niña the subtropical jet stream is displaced southward (Drosdowsky 2003). Furthermore, the impact of a stronger SAM is thought to induce a poleward shift in the STR (Williams and Stone 2009). These studies, however, did not compare the relationship of the STRI with modes of climate variability. In particular, the influence of the IOD on the STR has been largely unexplored. As such, we examine the relationship between the STR with these three modes in the context of their relative impacts on Australian rainfall and the associated atmospheric conditions.

2. Data and method

Although the dynamics of rainfall reduction over SWWA and parts of SEA show possible linkages (Hope et al. 2009), we focus on the SEA region, rather than on all of southern Australia as in Larsen and Nicholls (2009). We utilize time series of STRI and STRP, which are calculated following the definition of Drosdowsky (2005), that is, using the area of 10°–44°S ,145°–150°E. The STRI is the maximum of the zonally averaged MSLP, whereas the STRP describes the latitude where the maximum occurs. Note that the latitude is expressed in terms of degrees south (a higher positive value indicates a higher latitude). To take into account the possibility that the dynamics for each season are different, all data are stratified into four seasons—austral summer, autumn, winter, and spring—rather than combining the winter and spring seasons or stratifying them into annual averages.

We focus on the period 1979–2008, when more reliable observations—particularly, satellite measurements—are available. The interpolated outgoing longwave radiation (OLR) gridded data from the National Oceanic and Atmospheric Administration (NOAA) are used to describe atmospheric convection (Liebmann and Smith 1996). The Met Office Hadley Centre Sea Ice and Sea Surface Temperature (HadISST) global reanalysis (Rayner et al. 2003) is used to construct indices of the IOD and ENSO and their patterns. Reanalyses from the National Centers for Environmental Prediction (NCEP) (Kalnay et al. 1996) are also used to examine the atmospheric circulation fields, such as MSLP, atmospheric vertical velocities, and geopotential height fields. Observed Australian rainfall data, subjected to extensive quality control from the Centre for Australian Weather and Climate Research (Jones

et al. 2009), are used to examine the IOD–rainfall and ENSO–rainfall relationships. Throughout this study, seasonal anomalies are constructed using the mean climate during the period 1979–2008, and all the time series are linearly detrended to eliminate any coherence generated by long-term trends.

For each season, ENSO is represented by Niño-3.4 (SST anomalies over 5°S–5°N, 170°–120°W), while the dipole mode index (DMI), defined by Saji et al. (1999), measures the temporal variations of the IOD. The DMI is the difference of SST anomalies averaged over the western pole of the IOD (IODW, 10°S–10°N, 50°–70°E) and eastern IOD region (IODE, 10°S–equator, 90°–110°E). The SAM is measured using an index described in Marshall (2003); it is based on MSLP observations only and avoids the bias in the high latitudes of the Southern Hemisphere seen in reanalysis products (e.g., Randel and Wu 1999; Marshall 2002; Marshall 2003).

Partial correlation and partial regression analysis, as used in Cai et al. (2011b), are conducted to examine the circulation anomalies associated with, for example, ENSO, after removing the covariance with the STRI and vice versa. For description purposes the corresponding indices are referred to as "NIÑO3.4$|_{\text{STRI}}$," that is, removing any covariance of the STRI with Niño-3.4 from the Niño-3.4 index.

The statistical significance of the anomalous circulation pattern associated with ENSO after "removing the STRI" may be described by a map of partial correlations [$C(x, y)$NIÑO-3.4$|_{\text{STRI}}$], which is calculated by removing the STRI coherent variance from gridpoint anomalies $A(x, y, t)$ to obtain the residual field $A(x, y, t)|_{\text{STRI}}$, and then correlating $A(x, y, t)|_{\text{STRI}}$ with NIÑO-3.4$|_{\text{STRI}}$. Likewise, a map of partial regression [$R(x, y)$NIÑO-3.4$|_{\text{STRI}}$] is constructed by regressing $A(x, y, t)|_{\text{STRI}}$ onto NIÑO-3.4$|_{\text{STRI}}$. It is important to note that removing the STRI in this manner also removes a portion of the ENSO signal that is coherent with the STRI. We also use a one-standard-deviation anomaly pattern to describe the size of anomalies. This is obtained by multiplying $R(x, y)$NIÑO-3.4$|_{\text{STRI}}$ with the standard deviation of NIÑO-3.4$|_{\text{STRI}}$. Such one-standard-deviation anomaly patterns facilitate a comparison of the size of anomalies associated with two indices with contrasting size (e.g., NIÑO-3.4$|_{\text{STRI}}$ and STRI$|_{\text{Niño3.4}}$ or NIÑO-3.4 and STRI). A comparison of regression coefficients alone often does not bring out such contrasts in the size.

3. Seasonality of the STR and the influence on Australian rainfall

The seasonal movement of the STR is worth emphasizing (Fig. 1a). After reaching a maximum intensity in June, the ridge migrates northward as the intensity decreases throughout much of July and August (see also Fig. 4 of Drosdowsky 2005). During summer, upon reaching a minimum in December, the ridge strengthens and migrates southward, reaching its southernmost latitude in February. In summer and winter, an increase in intensity tends to be associated with a higher latitudinal position, and vice versa (Figs. 1b and 1d). The relationship in spring and autumn is somewhat different: after reaching a northernmost latitude in September, the ridge moves southward as the intensity weakens during October and November but moves northward as the intensity increases during March–June.

TABLE 1. Seasonal correlations of STRI and STRP with Niño-3.4, DMI, SAM, and SEA rainfall over 1979–2008. All indices are detrended prior to calculation. The bold correlations indicate significance above the 95% confidence level. The DMI is excluded in summer and autumn because the IOD does not operate during those seasons.

	DJF		MAM		JJA		SON	
	STRI	STRP	STRI	STRP	STRI	STRP	STRI	STRP
Niño-3.4	0.23	0.02	0.26	−0.26	**0.39**	0.17	**0.48**	0.07
DMI					**0.65**	**0.44**	**0.55**	0.17
SAM	0.35	**0.37**	0.08	0.06	**0.41**	**0.36**	0.09	0.25
SEA rainfall	0.11	0.14	−0.35	0.22	**−0.78**	**−0.67**	**−0.53**	−0.23

In terms of anomalies, the STRP and the STRI are strongly coherent in the summer, winter, and spring seasons (Figs. 1b, 1d, and 1e, respectively), and they are statistically significant at the 95% confidence level ($r >$ 0.36): when the intensity is anomalously strong, the position is anomalously poleward, and vice versa. The STR position–intensity relationship is strongest in winter, in which the influence from the IOD and the SAM on STRI and STRP (Table 1) dominates. In spring, the position–intensity coherence is high, and the variations in the STRI are mainly influenced by ENSO and the IOD, although these two modes have little impact on the STRP (Table 1). In summer, the STRI-STRP coherence is still high and statistically significant at the 95% confidence level. Surprisingly, during autumn, there is no relationship between the anomalous STRI and STRP (Fig. 1c), suggesting that they are not influenced by a common forcing.

Williams and Stone (2009) have indicated that the correlation of SEA rainfall with the STRP is weak in summer and that there is no obvious trend in the STRP in this season (also see bottom panel of Fig. 2a; Table 1). Therefore, the slight summer SEA rainfall increase since 1979 (Table 2) seems unrelated to the STRP. In this season, the IOD does not operate, and the influence of ENSO on either the STRI or the STRP is weak with no obvious Southern Oscillation pattern in Fig. 2c.

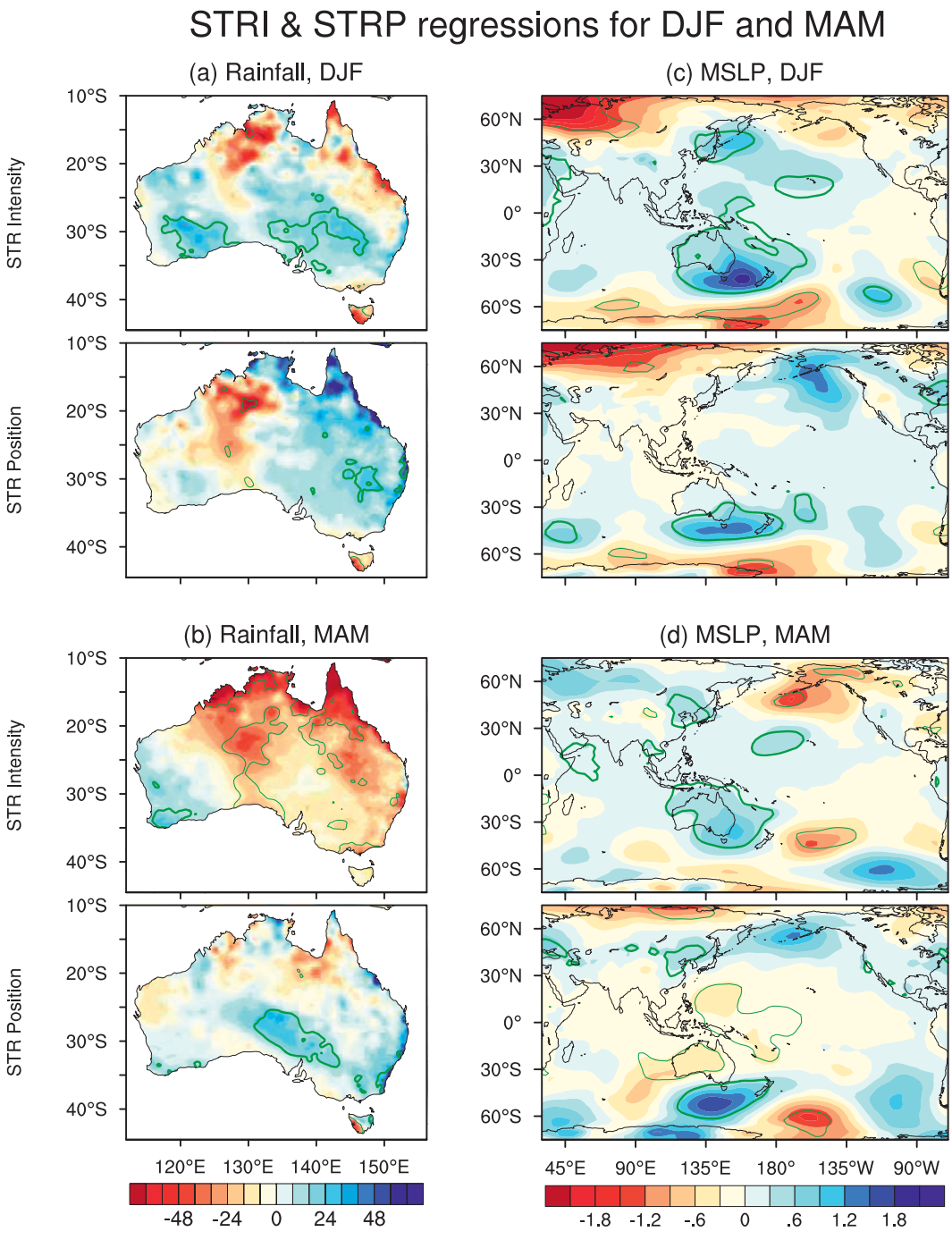

FIG. 2. One-standard-deviation anomaly rainfall patterns associated with the (top) STRI and (bottom) STRP for (a) summer and (b) autumn. (c),(d) As in (a),(b), but for MSLP anomalies. The thick (thin) green contours indicate positive (negative) significant correlations above the 95% confidence level.

In autumn, SEA rainfall (mostly over southern Victoria) is only weakly correlated with the STRI and the STRP (Fig. 2b), which discounts the utility of the ridge as a bridge to understand the dynamics of the large rainfall reduction in this season. Furthermore, there is virtually no impact of the SAM on the STR in this season (Table 1), which is verified in the MSLP pattern showing no SAM-like structure (Fig. 2d). In this season the IOD has not developed, while the influence of ENSO is weak (Table 1).

Because the STR is only significantly correlated with SEA rainfall in winter and spring, we focus on these two

TABLE 2. Seasonal trends of STRI, STRP, Niño-3.4, DMI, SAM, and SEA rainfall over 1979–2008. The standard errors are shown in italics. The significant trends, above the 95% confidence level, are shown in bold. The DMI is excluded in summer and autumn because the IOD does not operate during those seasons.

	STRI hPa (30 yr)$^{-1}$	STRP °C (30 yr)$^{-1}$	Niño-3.4 °C (30 yr)$^{-1}$	DMI °C (30 yr)$^{-1}$	SAM (30 yr)$^{-1}$	SEA rainfall mm (30 yr)$^{-1}$
DJF	0.97	1.08	−0.56		**1.68**	20.9
	±0.90	*±1.43*	*±0.68*		***±0.73***	*±22.6*
MAM	0.54	−0.04	−0.40		0.99	**−65.8**
	±0.62	*±0.85*	*±0.42*		*±0.69*	***±24.5***
JJA	1.21	1.34	−0.02	0.28	−0.11	−22.0
	±1.06	*±1.51*	*±0.40*	*±0.21*	*±0.69*	*±29.8*
SON	0.61	−0.88	−0.19	0.34	0.02	−14.0
	±0.71	*±1.70*	*±0.61*	*±0.25*	*±0.78*	*±27.9*

seasons and explore the influence of the three modes of variability on the STR.

4. Impact of modes of variability on the STR: Winter

During winter, both the STRI and STRP have a strong coherence with SEA rainfall (Figs. 3a and 3d, right column). The anomalies associated with the STRI and STRP show similar patterns and are comparable in size, while the circulation patterns have a strong imprint of a SAM-like pattern, similar to the southern Australian (local) pressure anomaly described in Lau and Nath (2004). This anomaly center south of Australia is found to be induced by an equivalent barotropic east Indian Ocean (EIO) wave train (Cai et al. 2011b). The wave train is a consequence of an extratropical response to convection anomalies and their associated anomalous upper-level divergence associated with the development of the IOD (Hoskins and Karoly 1981; Cai et al. 2011b); this is discussed further in the following sections. Removing the influence of STRP from the STRI greatly weakens the MSLP (not shown) and 200-hPa geopotential height anomalies, and it substantially reduces the STRI influence on southern Australia rainfall (Fig. 3b). Likewise, removing the impact of the STRI from the STRP leaves few anomalies (Fig. 3c), again highlighting the strong coherence between the two STR parameters in this season (Fig. 1d).

A comparison of Figs. 3b and 3c indicates the existence of possible linearly independent impacts from the STRI and STRP. For example, along Australia's east coast (to the east of the Great Dividing Range), their impacts are opposing. As shown previously, in winter, when the STRI is anomalously strong, the STRP tends to be located at higher latitudes (Fig. 1d). Although the high MSLP is not conducive to rainfall, the higher-latitude position could mean that more rain-bearing easterly systems are able to advect toward Australia's east coast (Pittock 1973). The two offsetting effects appear to be comparable in magnitude, resulting in a weak rainfall signal along the east coast (Fig. 3a). Because of the high coherence between the STRI and STRP, and a higher portion of rainfall covariance that the STRI represents, we only show results associated with the STRI; the results for the STRP are virtually identical, albeit slightly weaker in size.

a. Impact from the IOD

The presence of a significant influence from the IOD is illustrated in Fig. 4, through its removal from the STRI ($\mathrm{STRI}|_{\mathrm{DMI}}$, Fig. 4a) and through removing the STRI from the IOD ($\mathrm{DMI}|_{\mathrm{STRII}}$, Fig. 4b). This allows a direct comparison to circulation and rainfall anomalies associated with the STRI and the IOD (Figs. 3a and 4c, respectively). Several important features emerge. First, for $\mathrm{STRI}|_{\mathrm{DMI}}$, the residual circulation and rainfall anomaly pattern are similar but weaker in size to those associated with the STRI (cf. Figs. 4a and 3a). The weakening is consistent with notion that the IOD contributes to fluctuations in the STR; a positive IOD not only increases the STRI but also pushes the STR poleward (see also Table 1). Second, the IOD's impact is manifested through the STR; for $\mathrm{DMI}|_{\mathrm{STRI}}$, nearly all the circulation and rainfall anomalies over SEA disappear (Fig. 4b). However, the IOD's impact accounts for only a moderate amount of the total STRI variance; removing the influence of the IOD still leaves a large residual portion of variance (Fig. 4c).

How does the IOD conduct its influence on the STR? In winter, the IOD-related convection is dominated by the cooling anomaly in the eastern pole. The negative SST anomalies suppress convection and generate anomalous vertical motion; the associated anomalous divergence acts as a source of Rossby waves. In the tropics, the response is trapped and baroclinic (Gill 1980), yet in the extratropics it is equivalent-barotropic in the form of a steady Rossby wave train pattern extending poleward and eastward into the extratropical latitudes (Hoskins and Karoly 1981; Horel and Wallace 1981; Karoly 1989). The EIO wave train has a high pressure and geopotential height center south of Australia (Fig. 4c), which acts to weaken the rain-bearing westerly weather systems over this region

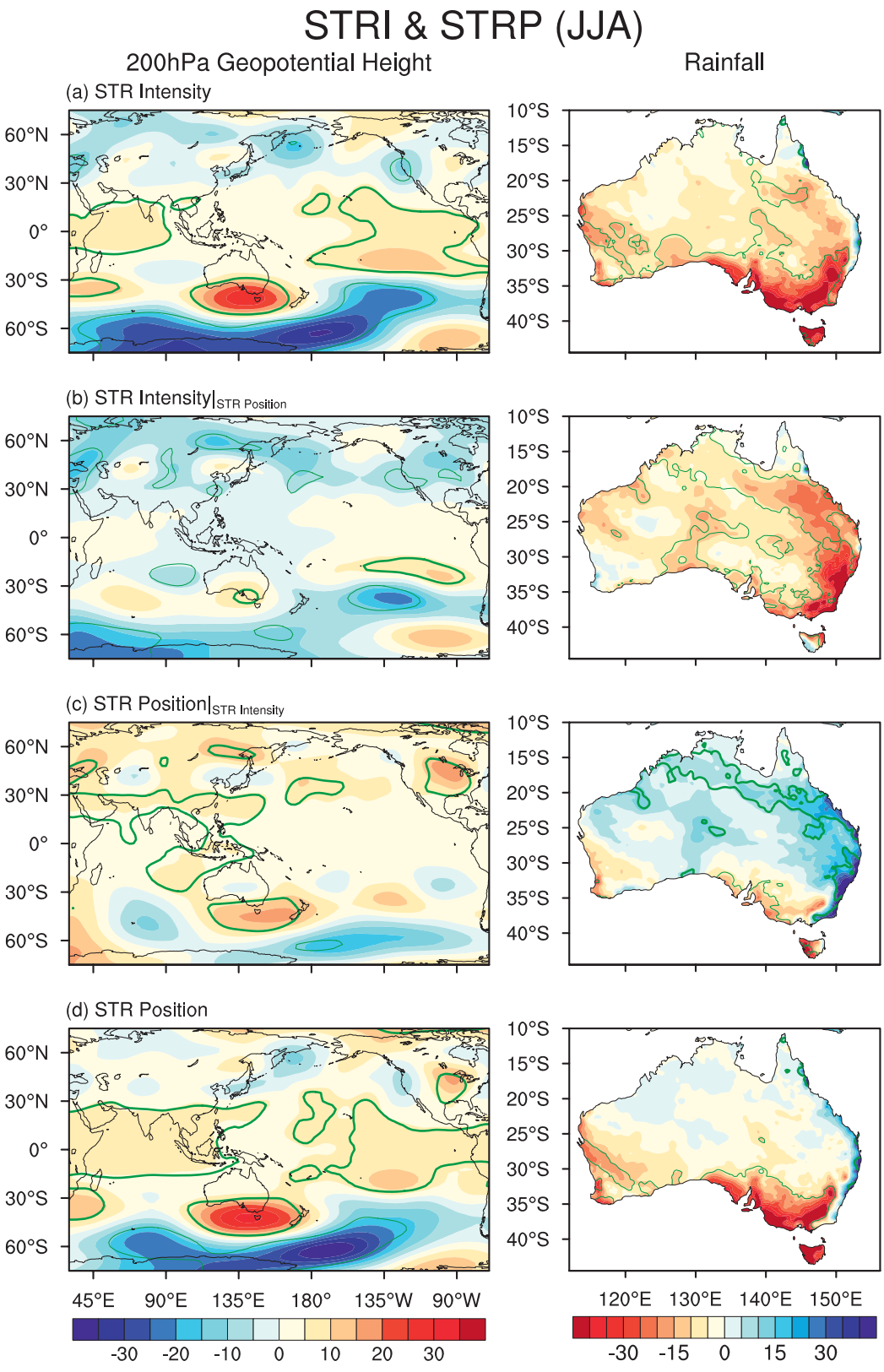

FIG. 3. One-standard-deviation winter anomalies of (left) 200-hPa geopotential height (m) and (right) Australian rainfall (mm) associated with (a) the STRI, (b) the STRI with the STRP removed, (c) the STRP with the STRI removed, and (d) the STRP. The green contours follow from the definition in Fig. 2.

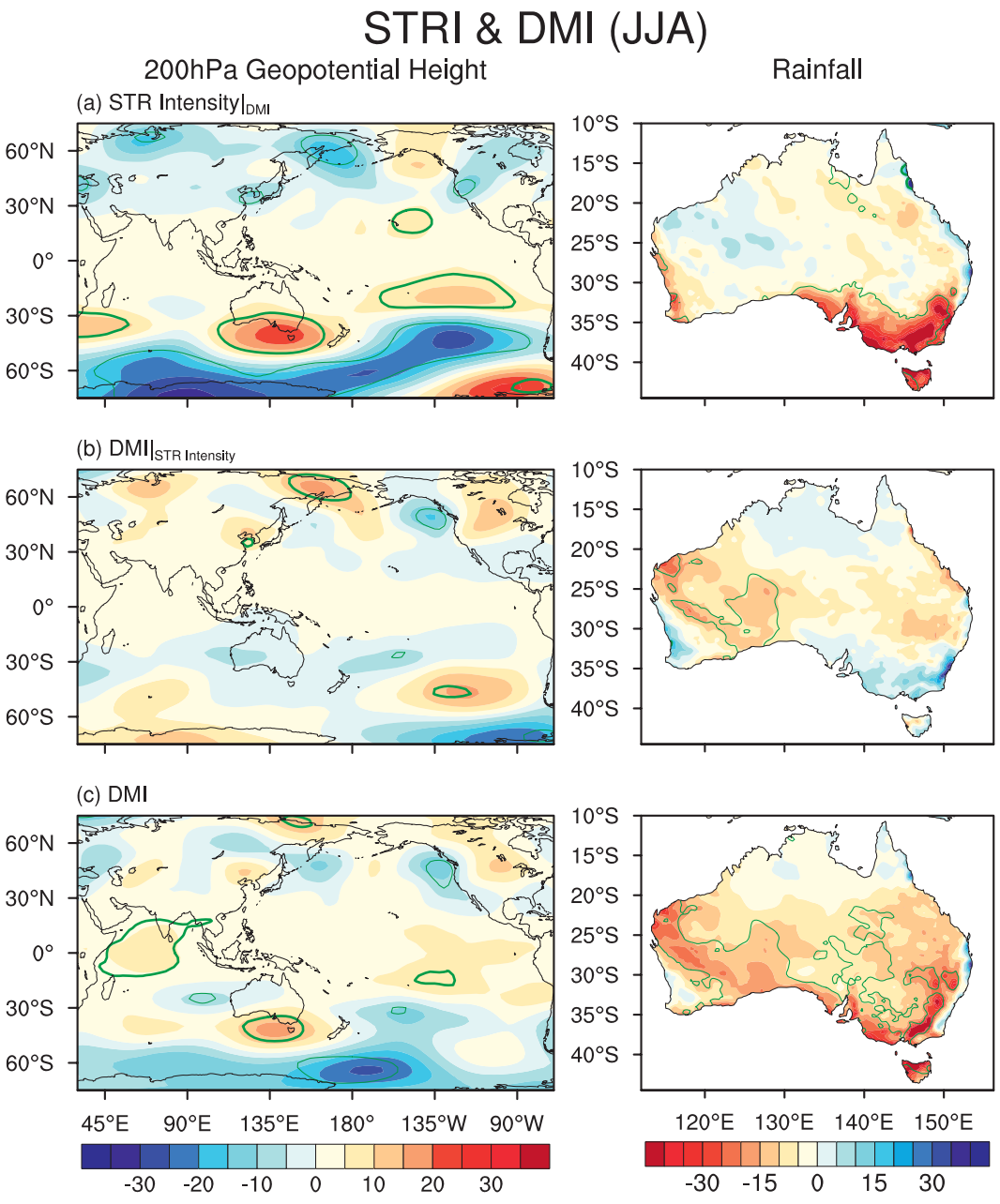

FIG. 4. One-standard-deviation winter anomalies of (left) 200-hPa geopotential height (m) and (right) Australian rainfall (mm) associated with (a) the STRI with the DMI removed (b) the DMI with STRI removed, and (c) the DMI. The green contours follow from the definition in Fig. 2.

[see Cai et al. (2011b) for further discussion]. Previous studies suggest that such a wave train mechanism is a process whereby the IOD generates temperature anomalies in regions that are remote to the IOD poles (Saji and Yamagata 2003; Saji et al. 2005).

b. *Impact from ENSO*

A similar plot reveals that there is virtually no impact from ENSO over SEA in the winter season (figure not shown). The extratropical wave train response to anomalous convection in the equatorial Pacific is mainly confined through the well-known Pacific–South American pattern and the Pacific–North American pattern. A wave train pattern originating from equatorial Africa (Cai et al. 2011b) is also observed, with significant positive MSLP anomalies over the southern Indian Ocean. However, none of these signals projects onto the STR. As such, removing ENSO from the STRI (STRI$|_{\text{ENSO}}$), or

vice versa ($ENSO|_{STRI}$), makes little difference to the associated anomalous circulation or rainfall patterns. In Table 1, ENSO displays a significant correlation with the STRI in winter; however, this appears to mainly reflect the changing MSLP around Australia, associated with the Darwin pole of the Southern Oscillation. While this can have an impact on rainfall across northern and eastern Australia through a tropical response, the impact on SEA rainfall is small. This is consistent with the findings of Cai et al. (2011b) who show that ENSO and the IOD are virtually independent in winter, with ENSO having little control on SEA rainfall during this season.

c. Influence from the SAM

Like the STR, the SAM shifts meridionally on an annual basis (Cai and Cowan 2006). In winter, the STR and the anomaly center of the SAM are located farthest from the equator. A higher midlatitude MSLP associated with a positive SAM induces a reduction in rainfall over SWWA and SEA (Fig. 5c), reinforcing the strong linkage in rainfall variations between the two regions (Hope et al. 2009). To investigate the role of the SAM impact conducted through the STRI, we remove the variance associated with the STRI ($SAM|_{STRI}$). The results (Fig. 5b) show that the SAM's impact is manifested through the STRI; without the STRI, the SAM's impact over southern Australia disappears (cf. Figs. 5b and 5c). Finally, the SAM's influence accounts for a small amount of the STRI variance, as evident in a comparison between Figs. 3a and 5a. Without the SAM ($STRI|_{SAM}$), the STRI impact on SEA and SWWA rainfall only slightly weakens; the impact through the STRP is similar but also slightly weaker.

To summarize, in winter an intensification of the STR is associated with it occurring in a higher latitudinal position. When the STR's extent is not as far northward as normal, the intensity tends to be higher, both leading to a reduction in SEA rainfall. The IOD and the SAM exert their impacts on SEA rainfall in this season, by projecting onto the STRI and STRP, linking the remote modes through changes in local atmospheric conditions.

5. Impact of modes of variability on the STR: Spring

During spring, only the STRI shows a significant impact on SEA and SWWA rainfall; however, the influence is weaker than that during winter (Table 1; cf Figs. 3a and 6a). In terms of the STRP, it has virtually no influence on SEA rainfall (Figs. 6c and 6d), and neither the IOD, ENSO, or the SAM is statistically coherent with the STRP (Table 1). This being the case, we again focus on the STRI for this season.

a. Impacts from the IOD

Removing the IOD (from the STRI) diminishes much of the covariance between the two climate modes, as well as substantially weakening the associated height anomalies south of Australia along with SEA and SWWA rainfall (cf. Figs. 7a and 6a). This highlights the importance of a large-scale climate driver, such as the IOD, in forcing remote responses in the extratropics. The impact is conducted via two Rossby wave trains (Fig. 7c): the EIO wave train as in winter and the other is referred to as the western Indian Ocean (WIO) wave train (Cai et al. 2011b). These two wave trains share a high pressure center south of Australia, and are the consequence of an extratropical response to the IOD-induced anomalous convection and divergence over the two IOD poles. As will be discussed later, the IOD influence contains a part that is driven by ENSO, because the Indian Ocean is an important pathway for ENSO's impact (Cai et al. 2011a,b).

How much of the IOD's impact is delivered through the STRI? Removing the STRI from the IOD eliminates most of the IOD impact over SEA and marginally weakens the IOD's impact on SWWA rainfall (cf. Figs. 7b and 7c). This suggests that not all of the IOD's impact is conducted through the STRI. This is because the STRI by definition has its center nearer to SEA, whereas the IOD-induced high pressure center south of Australia is situated farther to the west. The IOD-induced high pressure is in close proximity to SWWA and induces a reduction in rain-bearing westerly weather systems passing over this region.

The importance of the IOD as a forcing of the STR over SEA can be further understood in terms of the tropical SST and convection anomalies. The STRI is more coherent with SST anomalies over the IODE pole than over the western pole (Fig. 8a), similar to the situation in winter. There is also a high coherence between convection over the two IOD poles and the Pacific. As such, once the IOD-related anomalies are removed, much of the Indo-Pacific SST and convection anomalies diminish (Fig. 8b), supporting the argument that the extratropical impact from the tropical Indo-Pacific system is conducted through the IOD (discussed further in section 4a). Conversely, not all of the impact from Indo-Pacific variability projects onto the STR: upon removal of the STRI from the IOD, substantial SST and convection anomalies remain (figures not shown); this is consistent with the Rossby wave train patterns (Figs. 7b and 7c).

b. Impact from ENSO

Although ENSO's impact on northern and eastern Australia during spring is conducted through a reduction

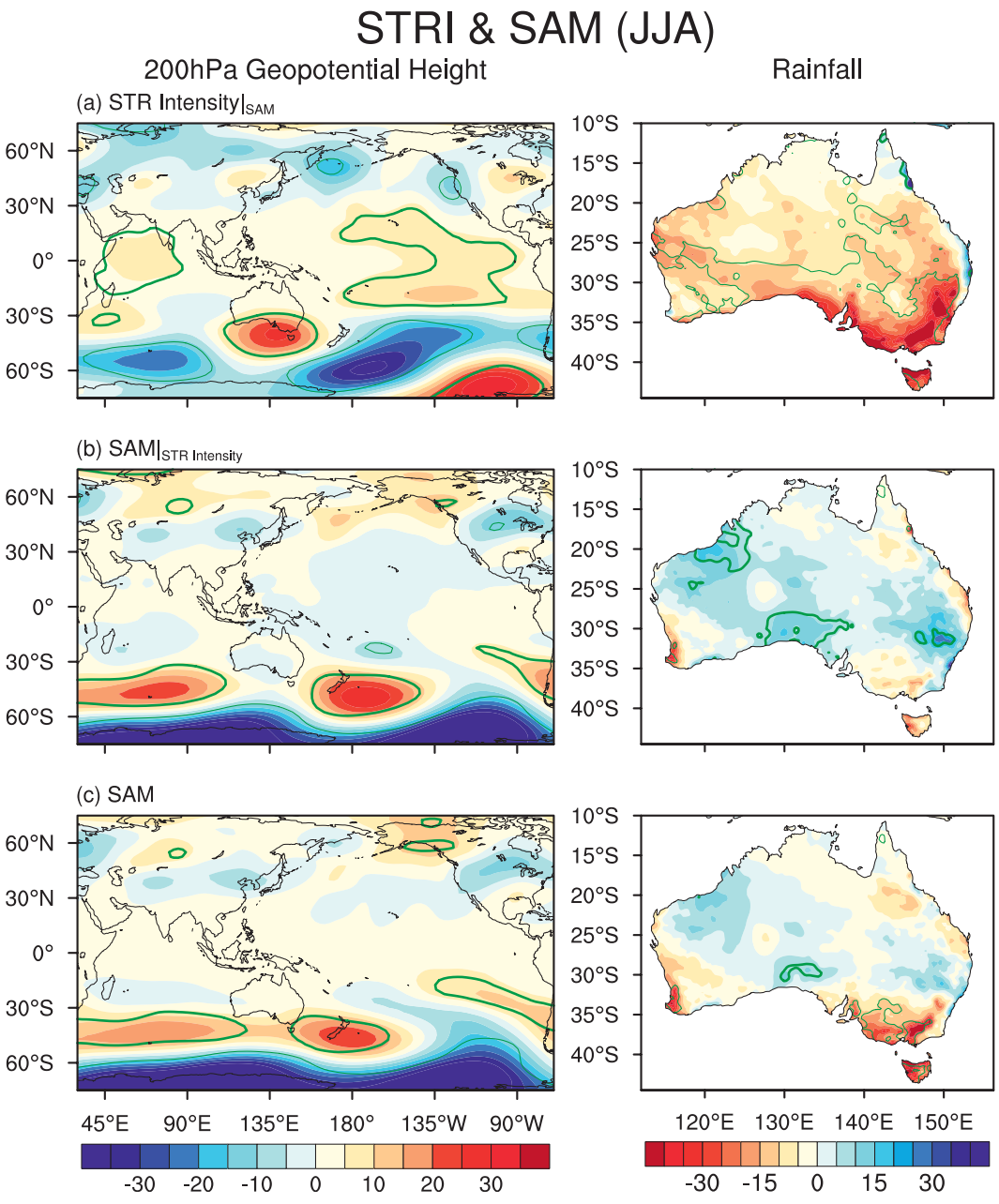

FIG. 5. As in Fig. 4, but the fields are associated with (a) STRI with the SAM index removed, (b) the SAM index with the STRI removed, and (c) the SAM.

in tropical convection over the western Pacific (Figs. 9b and 9c), ENSO's impact on southern Australia is conducted through the Indian Ocean (Cai et al. 2011b). As an El Niño develops, atmospheric convection over the western Pacific shifts eastward toward the date line. This suppresses rainfall and induces easterly anomalies in the equatorial EIO (e.g., Saji et al. 1999; Cai et al. 2005), contributing to the cooling in the IODE through two processes. First, because the climatological mean winds are easterly south of the equator during spring, the induced easterlies act to increase the wind speed and the latent and sensible heat fluxes, conducive to a cooling in the east. Second, shoaling of the thermocline and upwelling of colder subsurface water are promoted off the Sumatra–Java coast, further contributing to the cooling. In the western portion of the basin, warm anomalies develop as the equatorial thermocline deepens in response to easterly anomalies. Further, an off-equatorial depression

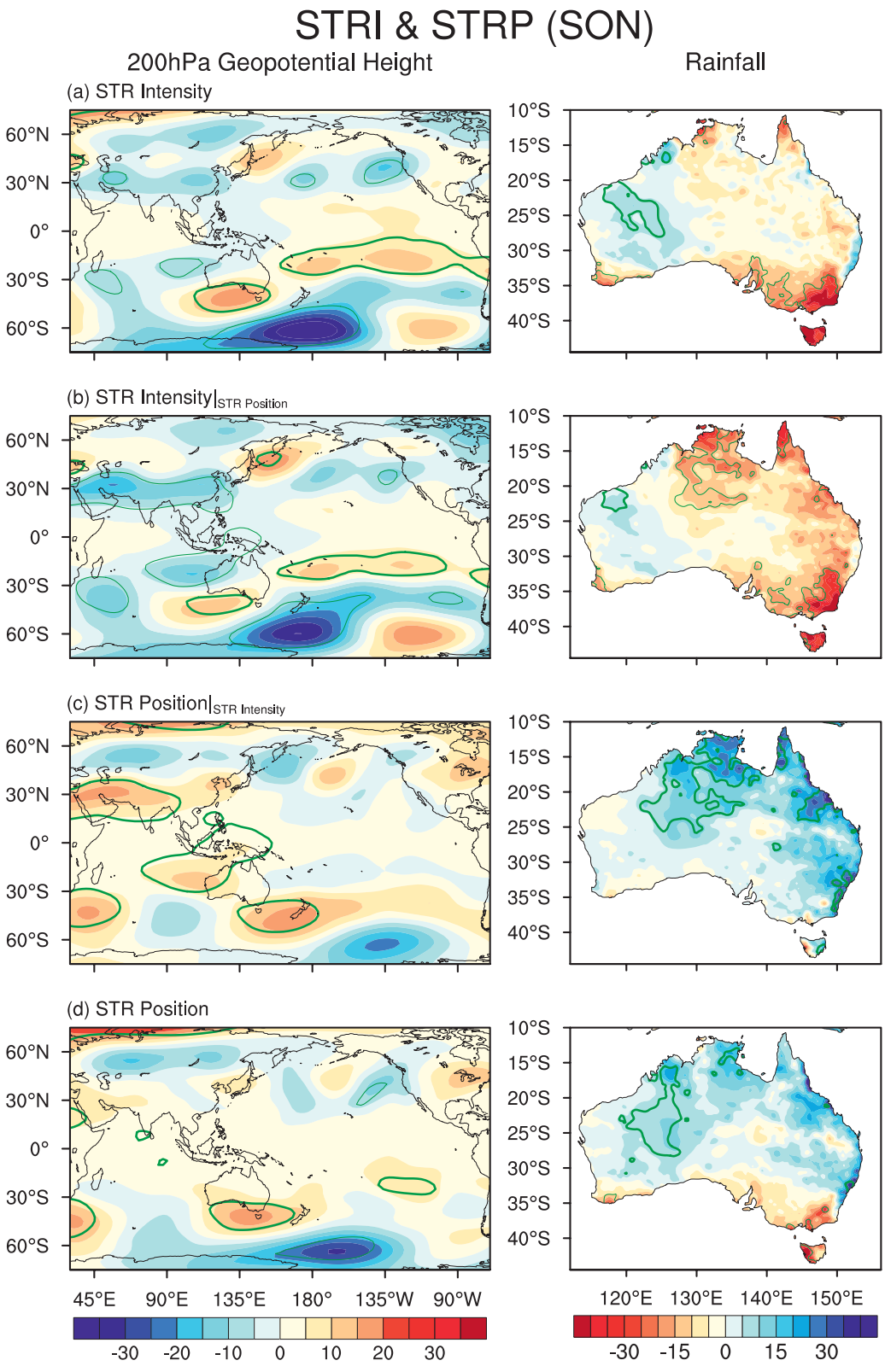

FIG. 6. As in Fig. 3, but for spring.

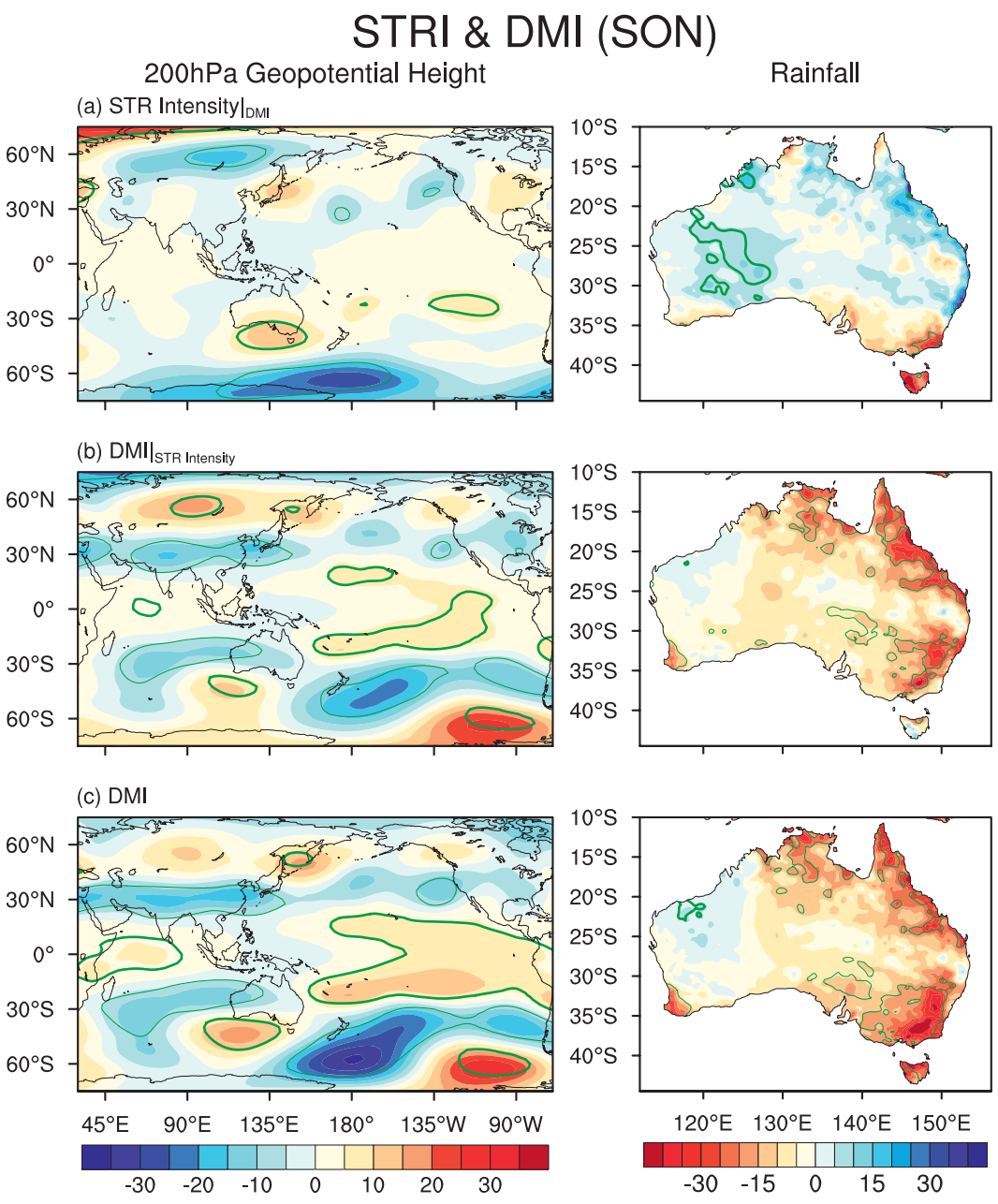

FIG. 7. As in Fig. 4, but for spring.

of the thermocline forced by Ekman pumping develops and propagates westward as an oceanic forced downwelling Rossby wave, reflecting and enhancing the warming in the west (Chambers et al. 1999; Webster et al. 1999; Xie et al. 2002). Thus, an El Niño contributes to the convection anomalies of the two IOD poles, exerting an impact on southern Australia through the WIO and EIO wave trains. The process is reflected in Fig. 9; removing ENSO's influence on the STRI (cf. Figs. 9a and 6a), or disabling the pathway via the STRI (cf. Figs. 9b and 9c), makes a distinct difference in ENSO's impact on southern Australia rainfall.

c. *Impacts from the SAM*

The SAM has very little impact on the STRI in spring (Table 1). It is worth emphasizing that during this season, a positive SAM is associated with stronger rainfall along the entire eastern Australia coast and the northern part of SEA because of an enhancement in the rain-bearing easterly weather systems. Over these regions the

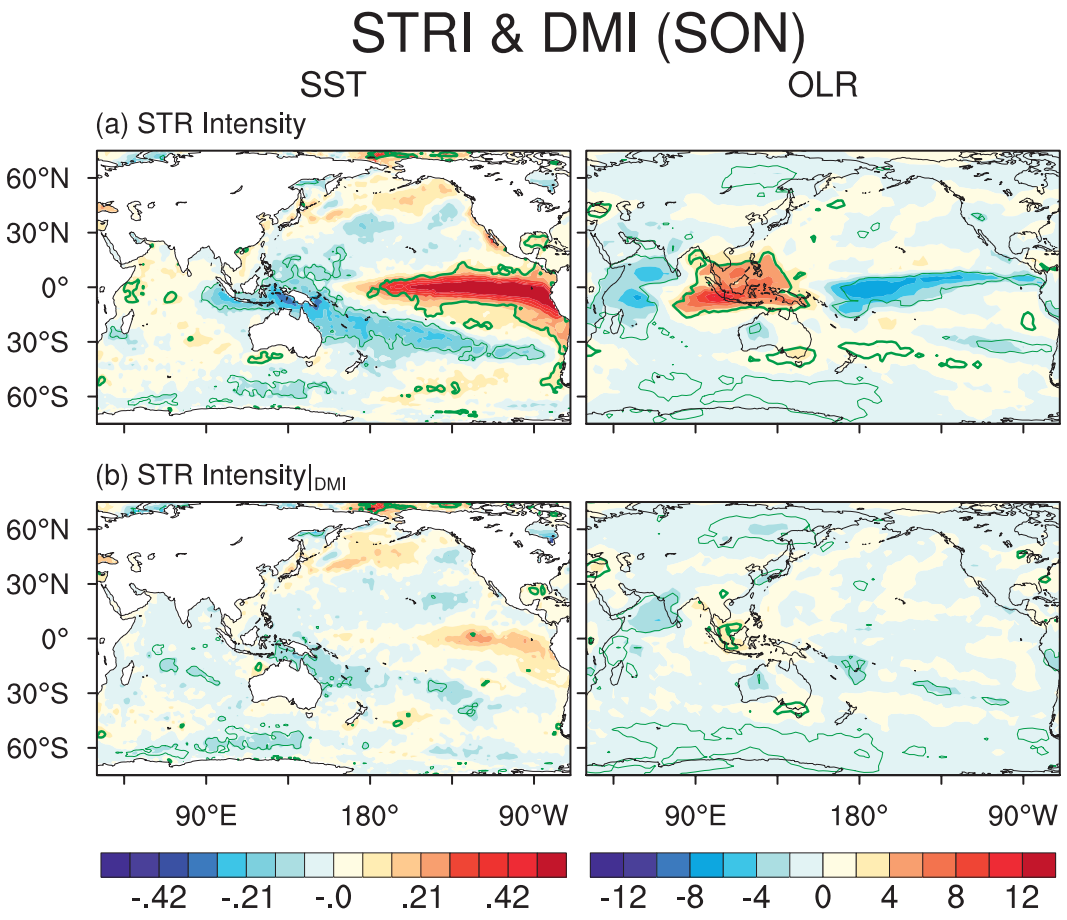

FIG. 8. One-standard-deviation spring anomalies of (left) SST (°C) and (right) OLR (W m^{-2}) associated with (a) STRI and (b) STRI with the DMI removed. The green contours follow from the definition in Fig. 2.

SAM explains between 10% and 15% of the weekly precipitation variability, comparable to ENSO (Hendon et al. 2007). The SAM tends to offset the influence of the STRI over southern SEA; as a result, once the impact of the SAM is removed, the STRI influence is slightly broader in scale but also stronger. However, the overall impact from the SAM on SEA is rather weak (figure not shown).

6. Implications for the dynamics of rainfall reduction

Having described the relationship between the major climate modes and the STR, we now discuss the potential role of their trends in STR changes and in the SEA rainfall reduction, assuming that relationships that operate interannually also occur on multidecadal time scales. Trends over the 1979–2008 period are listed in Table 2. It is immediately clear that only the SEA rainfall reduction in autumn and the SAM trend in summer are statistically significant at the 95% confidence level.

Despite the large reduction in SEA autumn rainfall, there is no commensurate trend in the STRI, consistent with the weak rainfall–STRI correlation (Table 1). These features reinforce the notion that the STRI is able to explain the large rainfall reduction in autumn. To further confirm this, we examine the sensitivity of SEA rainfall to the STRI (Fig. 10). For autumn, this sensitivity is -13.7 ± 6.9 mm hPa^{-1}. The total trend in the STRI over the 30-yr period is 0.54 ± 0.62 hPa, meaning that the total autumn rainfall reduction that can be attributed to the STRI is about 7.4 mm, or 11% of the observed trend. There is no obvious cause for the small STRI trend in this season; as a result, the dynamics of the SEA autumn rainfall decline remain elusive.

During winter, there is a substantial reduction in SEA rainfall as shown in the bottom left panel of Fig. 11 (also Table 2). The sensitivity of winter rainfall to the STRI is -21.9 ± 3.3 mm hPa^{-1}, with the trend in the STRI [1.2 ± 1.1 hPa $(30\ yr)^{-1}$] potentially accounting for more than the rainfall reduction (22 mm in 30 yr). However, the large error range in the STRI trend (±30 mm) should

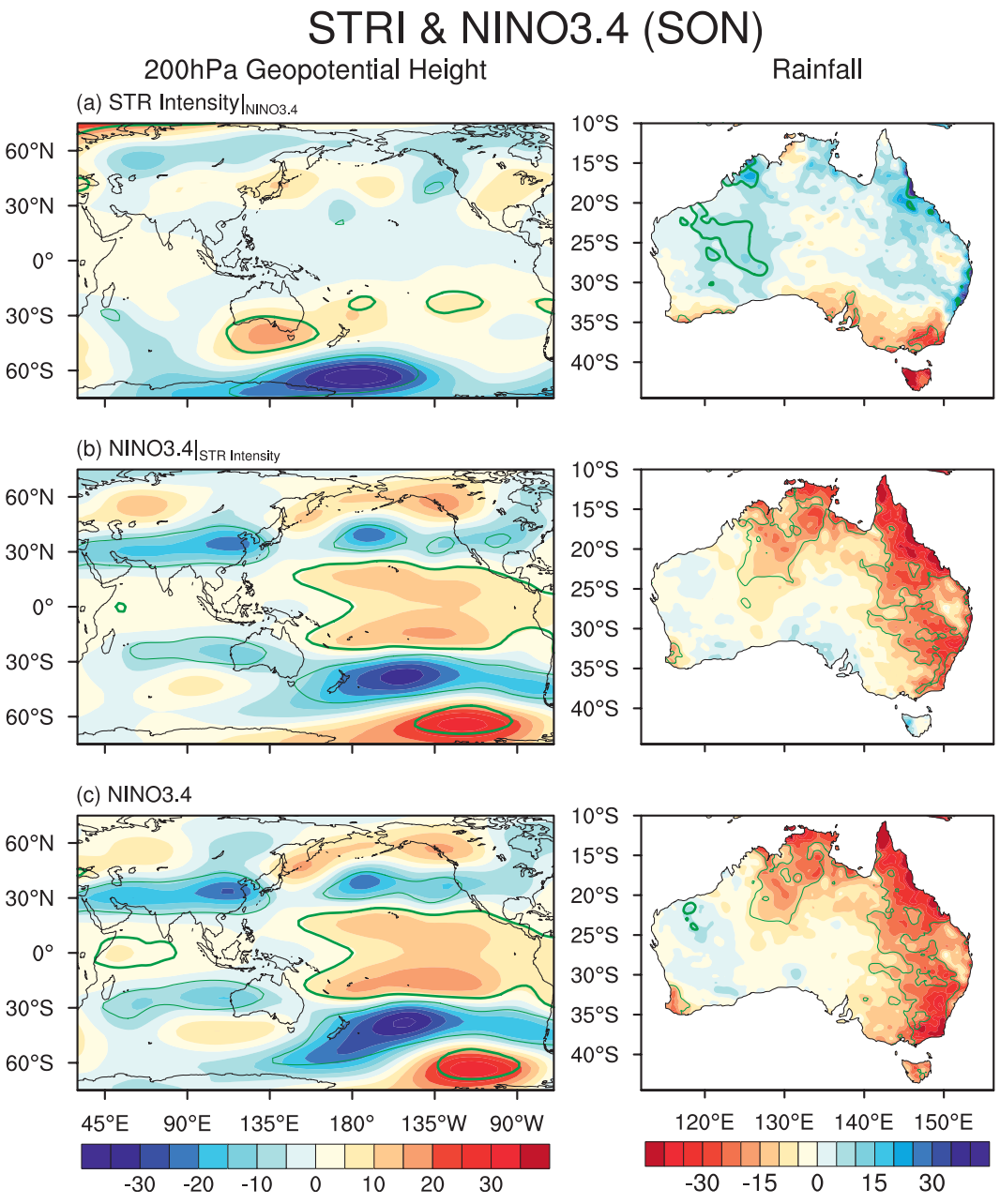

FIG. 9. One-standard-deviation spring anomalies of (left) 200-hPa geopotential height (m) and (right) Australian rainfall (mm) associated with (a) the STRI with ENSO removed, (b) ENSO with the STRI removed, and (c) ENSO. The green contours follow from the definition in Fig. 2.

be taken into account. Both the IOD and the SAM affect the STR in winter; however, there is no positive trend in the SAM (Fig. 11; Table 2). Therefore, the SAM cannot be considered a forcing factor for the winter rainfall decline. In recent decades the IOD has been trending upward (Fig. 11), manifested as a strong increase in the number of positive IOD events, while the number of negative IOD events has decreased (Cai et al. 2009b; Ummenhofer et al. 2009; Ummenhofer et al. 2011). In fact, from 2002 to 2009, there were five positive IOD events (2002, 2004, 2006, 2007, 2008) but only one weak negative event in 2009.[1] Further, over the past 30 years a total of 10 positive IOD events have occurred compared with a frequency of only two in the first 30 years of the twentieth century (Cai et al. 2009b). Thus, the IOD

[1] A negative IOD event occurred in 2010.

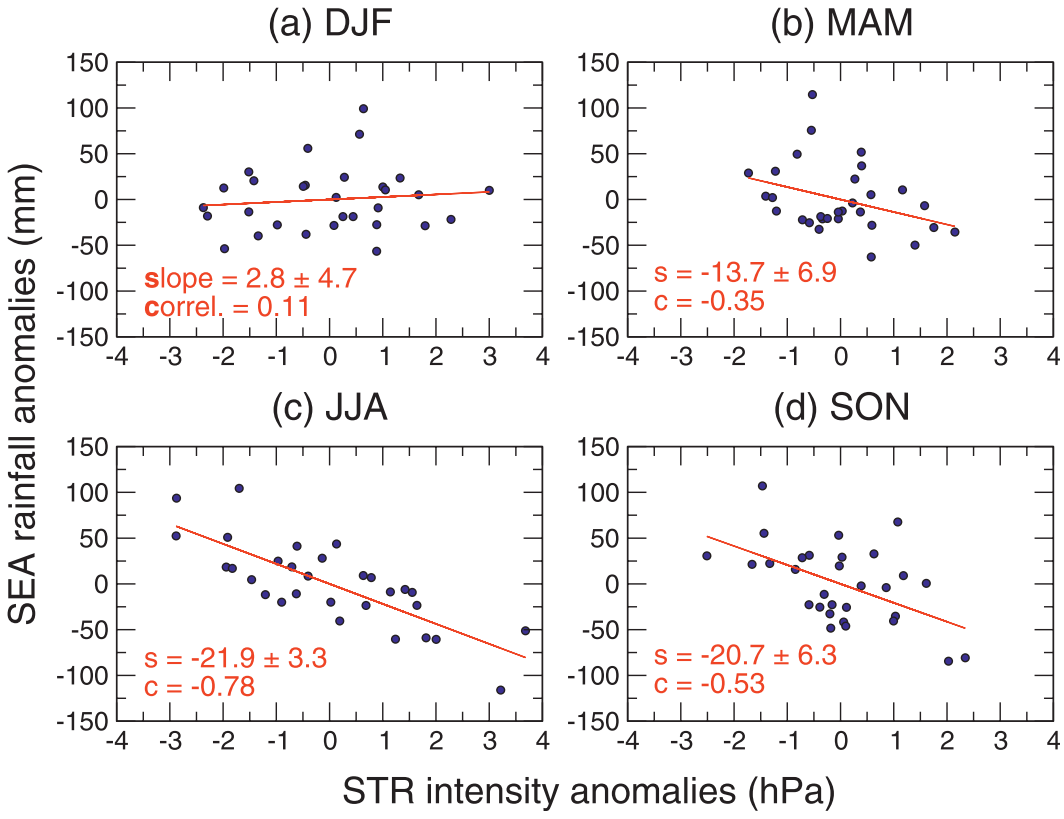

FIG. 10. Scatterplot of detrended SEA rainfall anomalies (mm) with detrended STRI anomalies (hPa) for (a) summer, (b) autumn, (c) winter, and (d) spring. The red line is the linear fit between the points.

trend is consistent with the rainfall reduction during winter. The sensitivity of SEA rainfall to the IOD is -61.9 ± 24.1 mm °C^{-1}, while the IOD trend is 0.28 ± 0.21°C (30 yr)$^{-1}$, giving a total median trend attributable to the IOD of -17.3 mm (30 yr)$^{-1}$, or about 79% of the total winter rainfall trend. Using twentieth-century experiments submitted to the Fourth Assessment Report of the Intergovernmental Panel on Climate Change, Cai et al. (2009a) argued that the increased frequency in positive IODs is consistent with the Indian Ocean's response to climate change. Therefore, the winter rainfall reduction may be interpreted as partially induced by climate change.

During spring, the sensitivity of rainfall to the STRI is -20.7 ± 6.3 mm hPa^{-1} (Fig. 10d), and with a trend of 0.6 ± 0.7 hPa (30 yr)$^{-1}$, the STRI accounts for a rainfall reduction of 12.4 mm (30 yr)$^{-1}$, or almost 90% of the total rainfall trend. The SAM has little impact on the STR or SEA rainfall in the spring season; therefore, it is unlikely to play a significant role in driving the small reduction in SEA spring rainfall. ENSO exerts an impact on SEA rainfall through the EIO and WIO wave trains; however, as there is very little trend in the ENSO index (Fig. 11; Table 2), it follows that ENSO is unlikely to be a forcing factor either. As the IOD has been trending up in recent decades, it is a possible contributor to the spring rainfall decline. The sensitivity of SEA rainfall to the IOD is -60.4 ± 17.8 mm °C^{-1}, and the IOD is trending up at 0.34 ± 0.25°C (30 yr)$^{-1}$. This gives rise to a rainfall trend of -20.5 mm (30 yr)$^{-1}$ that is accounted for by the IOD trend, an amount that is greater than the total SEA spring rainfall reduction. We note, however, that interannual variability in ENSO (Fig. 11) would provide some offset to the IOD-induced rainfall trend.

7. Conclusions

Numerous studies have explored the linkage between the STR and southern Australia rainfall, mostly by focusing on the influence of the ridge position. A motivation for examining the linkage is that by identifying factors that contribute to variability and trends of the STR, one may unravel the cause of the observed rainfall reduction. It is particularly hoped that such an approach would eventually lead to an explanation for the SEA autumn rainfall reduction, which is the largest of all seasons and critical for "wetting" the soil ahead of the main rainfall months.

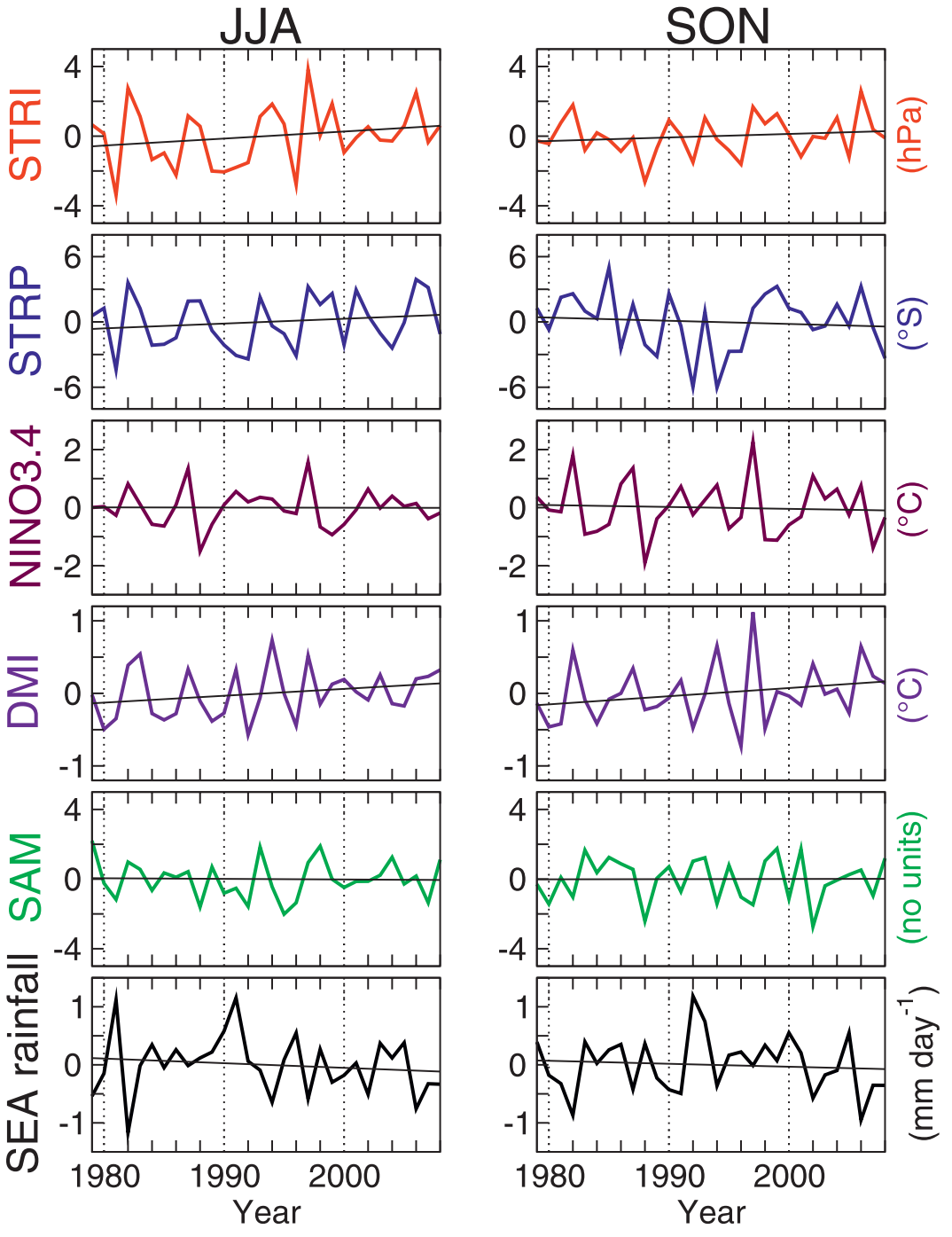

FIG. 11. Time series of local and remote climate drivers, including SEA rainfall over 1979–2008 (shown as anomalies over this period) for winter and spring. The units are shown on the right-hand side of the plot. A linear trend line is also plotted with the slope and standard error values listed in Table 2.

We have examined the influence of three major climate modes on both the position and the intensity of the STR over the SEA region. We find that there is no obvious utility of such an approach for autumn because the modes of variability, such as the SAM and ENSO, do not influence the STR (the IOD does not operate in this season). This result is predetermined by the fact that the STRI and STRP are poor surrogates for SEA rainfall in autumn: their correlation with rainfall is much lower in autumn than in winter or spring. As such, the autumn

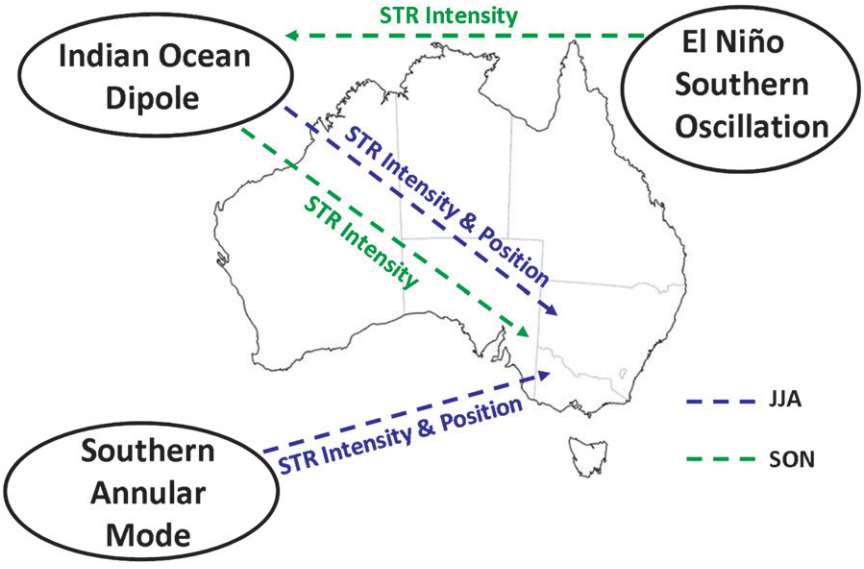

FIG. 12. Schematic showing the impact of climate drivers on the STR in winter (blue arrows) and in spring (green arrows). In winter, the IOD and the SAM influence the STR through both the intensity and the position. In spring, both the IOD and ENSO have an impact on the intensity; however, the impact of ENSO is conducted through the IOD (e.g., Cai et al. 2011b). A further detailed explanation is provided in the text.

SEA rainfall reduction is by and large not reflected in either the intensity or the position of the STR. Indeed, the STRI accounts for only around 11% of the total autumn rainfall reduction.

The highest utility is seen in winter, when the STRI and STRP are highly congruent and good surrogates for SEA rainfall. In this season, an anomalous STR poleward movement is associated with a strengthening STRI. The impact of the three climate drivers on the winter STR is summarized in Fig. 12 (blue arrows). A positive IOD or a positive SAM increases the STR intensity and pushes the ridge poleward. The IOD impact is conducted through an equivalent-barotropic EIO wave train, which has a high pressure center in good alignment with the STR over SEA. With this being the case, the IOD's impact is manifested through the STR. There is no significant trend in the SAM (Table 2). The STR trend accounts for the entire observed winter rainfall reduction since 1979, with 80% of the STRI-induced rainfall trend contributed by the IOD.

In spring, the STR is a good surrogate for SEA rainfall. The influence of the SAM is weak, while major drivers, such as the IOD and ENSO, are strong (they show strong covariations) and exert their impact on the STRI. In this season, the Indian Ocean is a primary source of ENSO's influence on SEA rainfall (Fig. 12, green arrows). The impact is conducted through WIO and EIO wave trains that share a pressure center south of Australia. However, the pressure center does not align with the STRI center. The upward IOD trend in this season, as observed in the DMI, accounts for a greater rainfall reduction than what has been observed; however, the IOD's impact appears to be offset by a weak decreasing trend in ENSO (as represented by Niño-3.4). The STRI trend accounts for 90% of the observed rainfall trend since 1979, all attributable to the upward trend in the IOD.

Our study has unraveled interacting processes whereby modes of climate variability in winter and spring exert their presence on the STR. Although a direct linkage between SEA rainfall and climate drivers is desirable, there is some utility of using the STR as a bridge to understand the dynamics of SEA rainfall variations and the recent reduction. However, in autumn, the approach offers no progress toward revealing the cause of the strong decline in SEA rainfall. An analysis using monthly stratified data is underway to examine the robustness of this conclusion. Preliminary results suggest that the STR–rainfall relationship varies vastly from month to month, and that there is a strong temporal variation on decadal time scales. These and the associated dynamics will be further explored in a future study.

Acknowledgments. This research is supported by the Australian Climate Change Science Program and the South East Australia Climate Initiative. We thank Bertrand Timbal and Wasyl Drosdowsky for providing time series of the subtropical ridge, and David Kent for reviewing the manuscript before submission. We are

grateful to Todd Mitchell and two anonymous reviewers for their helpful comments.

REFERENCES

Ashok, K., Z. Guan, and T. Yamagata, 2003: Influence of the Indian Ocean dipole on the Australian winter rainfall. *Geophys. Res. Lett.,* **30,** 1821, doi:10.1029/2003GL017926.

Cai, W., and T. Cowan, 2006: SAM and regional rainfall in IPCC AR4 models: Can anthropogenic forcing account for southwest Western Australian winter rainfall reduction? *Geophys. Res. Lett.,* **33,** L24708, doi:10.1029/2006GL028037.

——, and ——, 2008a: Dynamics of late autumn rainfall reduction over southeastern Australia. *Geophys. Res. Lett.,* **35,** L09708, doi:10.1029/2008GL033727.

——, and ——, 2008b: Evidence of impacts from rising temperature on inflows to the Murray-Darling Basin. *Geophys. Res. Lett.,* **35,** L07701, doi:10.1029/2008GL033390.

——, P. H. Whetton, and D. J. Karoly, 2003: The response of the Antarctic Oscillation to increasing and stabilized atmospheric CO_2. *J. Climate,* **16,** 1525–1538.

——, H. H. Hendon, and G. Meyers, 2005: Indian Ocean dipolelike variability in the CSIRO Mark 3 coupled climate model. *J. Climate,* **18,** 1449–1468.

——, T. Cowan, and M. Raupach, 2009a: Positive Indian Ocean dipole events precondition southeast Australia bushfires. *Geophys. Res. Lett.,* **36,** L19710, doi:10.1029/2009GL039902.

——, ——, and A. Sullivan, 2009b: Recent unprecedented skewness towards positive Indian Ocean dipole occurrences and its impact on Australian rainfall. *Geophys. Res. Lett.,* **36,** L11705, doi:10.1029/2009GL037604.

——, A. Sullivan, and T. Cowan, 2011a: Interactions of ENSO, the IOD, and the SAM in CMIP3 models. *J. Climate,* **24,** 1688–1704.

——, P. van Rensch, T. Cowan, and H. H. Hendon, 2011b: Teleconnection pathways of ENSO and the IOD and the mechanisms for impacts on Australian rainfall. *J. Climate,* **24,** 3910–3923.

Chambers, D. P., B. D. Tapley, and R. H. Stewart, 1999: Anomalous warming in the Indian Ocean coincident with El Niño. *J. Geophys. Res.,* **104,** 3035–3047.

Chen, G., J. Lu, and D. M. W. Frierson, 2008: Phase speed spectra and the latitude of surface westerlies: Interannual variability and global warming trend. *J. Climate,* **21,** 5942–5959.

Drosdowsky, W., 2003: An analysis of Australian seasonal rainfall and teleconnection patterns anomalies: 1950–1987. II: Temporal variability. *Int. J. Climatol.,* **13,** 111–149.

——, 2005: The latitude of the subtropical ridge over eastern Australia: The L-index revisited. *Int. J. Climatol.,* **25,** 1291–1299.

Gallant, A. J. E., K. J. Hennessy, and J. Risbey, 2007: Trends in rainfall indices for six Australian regions: 1910–2005. *Aust. Meteor. Mag.,* **56,** 223–239.

Gibson, T. T., 1992: An observed poleward shift of the Southern Hemisphere subtropical wind maximum—A greenhouse symptom? *Int. J. Climatol.,* **12,** 637–640.

Gill, A. E., 1980: Some simple solutions for heat-induced tropical circulation. *Quart. J. Roy. Meteor. Soc.,* **106,** 447–462.

Hendon, H. H., D. W. J. Thompson, and M. C. Wheeler, 2007: Australian rainfall and surface temperature variations associated with the Southern Hemisphere annular mode. *J. Climate,* **20,** 2452–2467.

Hope, P., B. Timbal, and R. Fawcett, 2009: Associations between rainfall variability in the southwest and southeast of Australia and their evolution through time. *Int. J. Climatol.,* **30,** 1360–1371, doi:10.1002/joc.1964.

Horel, J. D., and J. M. Wallace, 1981: Planetary-scale atmospheric phenomena associated with the Southern Oscillation. *Mon. Wea. Rev.,* **109,** 813–829.

Hoskins, B. J., and D. J. Karoly, 1981: The steady linear response of a spherical atmosphere to thermal and orographic forcing. *J. Atmos. Sci.,* **38,** 1179–1196.

Jones, D. A., W. Wang, and R. Fawcett, 2009: High-quality spatial climate data-sets for Australia. *Aust. Meteor. Oceanogr. J.,* **58,** 233–248.

Kalnay, E., and Coauthors, 1996: The NCEP/NCAR 40-Year Reanalysis Project. *Bull. Amer. Meteor. Soc.,* **77,** 437–471.

Karoly, D. J., 1989: Southern Hemisphere circulation features associated with El Niño–Southern Oscillation events. *J. Climate,* **2,** 1239–1252.

Larsen, S. H., 2008: Australian winter anticyclonicity, 1850–2006. *J. Geophys. Res.,* **113,** D06105, doi:10.1029/2007JD008873.

——, and N. Nicholls, 2009: Southern Australian rainfall and the subtropical ridge: Variations, interrelationships, and trends. *Geophys. Res. Lett.,* **36,** L08708, doi:10.1029/2009GL037786.

Lau, N.-C., and M. J. Nath, 2004: Coupled GCM simulation of atmosphere–ocean variability associated with zonally asymmetric SST changes in the tropical Indian Ocean. *J. Climate,* **17,** 245–265.

Li, Y., W. Cai, and E. P. Campbell, 2005: Statistical modeling of extreme rainfall in southwest Western Australia. *J. Climate,* **18,** 852–863.

Liebmann, B., and C. A. Smith, 1996: Description of a complete (interpolated) outgoing longwave radiation dataset. *Bull. Amer. Meteor. Soc.,* **77,** 1275–1277.

Marshall, G. J., 2002: Trends in Antarctic geopotential height and temperature: A comparison between radiosonde and NCEP–NCAR reanalysis data. *J. Climate,* **15,** 659–674.

——, 2003: Trends in the southern annular mode from observations and reanalyses. *J. Climate,* **16,** 4134–4143.

McBride, J. L., and N. Nicholls, 1983: Seasonal relationships between Australian rainfall and the Southern Oscillation. *Mon. Wea. Rev.,* **111,** 1998–2004.

Murphy, B., and B. Timbal, 2008: A review of recent climate variability and climate change in south-eastern Australia. *Int. J. Climatol.,* **28,** 859–879.

Pittock, B., 1973: Global meridional interactions in stratosphere and troposphere. *Quart. J. Roy. Meteor. Soc.,* **99,** 424–437.

Randel, W. J., and F. Wu, 1999: Cooling of the Arctic and Antarctic polar stratospheres due to ozone depletion. *J. Climate,* **12,** 1467–1479.

Rayner, N. A., D. E. Parker, E. B. Horton, C. K. Folland, L. V. Alexander, D. P. Rowell, E. C. Kent, and A. Kaplan, 2003: Global analyses of sea surface temperature, sea ice, and night marine air temperature since the late nineteenth century. *J. Geophys. Res.,* **108,** 4407, doi:10.1029/2002JD002670.

Ropelewski, C. F., and M. S. Halpert, 1987: Global and regional scale precipitation patterns associated with the El Niño/Southern Oscillation. *Mon. Wea. Rev.,* **115,** 1606–1626.

Saji, N. H., and T. Yamagata, 2003: Possible impacts of Indian Ocean dipole mode events on global climate. *Climate Res.,* **25,** 151–169.

——, B. N. Goswami, P. N. Vinayachandran, and T. Yamagata, 1999: A dipole mode in the tropical Indian Ocean. *Nature,* **401,** 360–363.

——, T. Ambrizzi, and S. E. T. Ferraz, 2005: Indian Ocean dipole mode events and austral surface air temperature anomalies. *Dyn. Atmos. Oceans,* **39,** 87–101.

Taschetto, A. S., and M. H. England, 2009: An analysis of late twentieth century trends in Australian rainfall. *Int. J. Climatol.,* **29,** 791–807.

Timbal, B., B. Murphy, K. Braganza, H. Hendon, M. Wheeler, and C. Rakich, 2007: Final report for project 1.1.2: Comparing documented climate changes with those attributable to specific causes. South Eastern Australian Climate Initiative Tech. Rep., 19 pp.

——, and Coauthors, 2010: Understanding the anthropogenic nature of the observed rainfall decline across south-eastern Australia. CAWCR Tech. Rep. 26, 180 pp.

Ummenhofer, C. C., M. H. England, P. C. McIntosh, G. A. Meyers, M. J. Pook, J. S. Risbey, A. Sen Gupta, and A. S. Taschetto, 2009: What causes southeast Australia's worst droughts? *Geophys. Res. Lett.,* **36,** L04706, doi:10.1029/2008GL036801.

——, and Coauthors, 2011: Indian and Pacific Ocean influences on southeast Australian drought and soil moisture. *J. Climate,* **24,** 1313–1336.

Webster, P. J., A. M. Moore, J. P. Loschnigg, and R. R. Leben, 1999: Coupled ocean-atmosphere dynamics in the Indian Ocean during 1997–98. *Nature,* **401,** 356–360.

Williams, A. A. J., and R. C. Stone, 2009: An assessment of relationships between the Australian subtropical ridge, rainfall variability, and high-latitude circulation patterns. *Int. J. Climatol.,* **29,** 691–709.

Wu, M. C., W. L. Chang, and W. M. Leung, 2004: Impacts of El Niño–Southern Oscillation events on tropical cyclone landfalling activity in the western North Pacific. *J. Climate,* **17,** 1419–1428.

Xie, S. P., H. Annamalai, F. A. Schott, and J. P. McCreary, 2002: Structure and mechanisms of south Indian Ocean climate variability. *J. Climate,* **15,** 864–878.

Yu, J., G. Fu, W. Cai, and T. Cowan, 2010: Impacts of precipitation and temperature changes on annual streamflow in the Murray-Darling basin. *Water Int.,* **35,** 313–323.